03-545 - Honors Research
Final Thesis Report

The Analysis of Colorectal Cancer Tumor-Stromal Interaction & the Optimization of a Testing Model

Joana Khatib

Carnegie Mellon University Qatar
Supervisor: Dr. Nesrine Affara

May 4th, 2021

Acknowledgements

First and foremost, praises and thanks to God for his blessings throughout my research, for endowing me the opportunity to learn, facilitating my educational journey and giving me the power to hopefully contribute.

I would like to thank Carnegie Mellon University in Qatar for providing with quality education, intriguing environment to grow in and introducing me to the faculty and staff who constructed my journey.

I would like to express my deep thanks to my research advisor Dr. Nesrine Affara for believing in me and giving me the opportunity to do the research, enrich my curiosity, and develop my lab skills.

I also would like to extend my gratitude to my advisory committee Dr. Anette Vincent and Dr. Mohamed Bouaouina, as well as all the Biological Sciences Faculty for their valuable feedback and continuous support.

I also want to acknowledge Weil Cornell Medical School in Qatar, and specifically Dr. Nasrin Mesaeli, for collaborating with us and helping us with the Trichrome staining the clinical samples.

To my parents and siblings, thank you for always being by my side and ahead of me paving the road, I would not be here without your love.

To my family, friends, lab colleague Fajer Al Marzooqi, and beloveds in Qatar, Syria, and the U.S., your unconditional and love was priceless!

Abstract. To halt the proliferation of cancer cells by leveraging their surroundings, a closer look at a proposed bi-directional relationship between the tumor and its stroma is studied. While previous research has established key factors within this mechanism such as TGF-β and SDF-1, we still lack the knowledge about the mechanism by which reprogramming occurs. Using HCT-116 immortalized colorectal cancer (CRC) cell lines and the readily available human foreskin fibroblasts (HFF), the reprogramming of fibroblast to cancer-associated fibroblasts is analyzed using 3D culture while optimizing an in-vivo like CRC model to be used for drug toxicity and further inter-relational studies. To address this endeavor, a co-culture of the mentioned cells was assessed for markers to better understand how the addition of naïve fibroblast affect the growth of tumor-derived spheroids. In return, the morphology of the naïve fibroblasts in comparison to that of an adenocarcinoma in addition to the protein expression change of fibroblasts when in the vicinity of a tumor were studied. Markers and number of fibroblasts were observed to increase due to tumor interaction. The tumor model was successfully optimized and studied to understands the micro (spheroids) to macro (in vivo tumor) translation.

Introduction

Colorectal cancer (CRC) is the third most common cancer in the world, and the second most common cause of cancer death in the U.S. [1]. In Qatar, CRC is the most prominent cancer type in men, and is second for women, after breast cancer [2]. CRC arises from malignant polyps in the inner linings of the colon or rectum caused by a disruption of the cell cycle where either a gain-of-function or loss-of-function mutation occurs in tumor suppressor gene, such as Adenomatous polyposis coli (APC) [3]. A mutation in APC interferes with downstream effectors including β-catenin, which is responsible for cell-cell adhesion and gene transcription, thus disrupts normal cell replication, migration, and adhesion [3]. Likewise, mutation in BRAF, KRAS, CTNNB1, p53, and particularly H-ras interrupt the signaling pathways, regulating cell cycle and growth, leading to a more aggressive phenotype [4]. While there are three major types of CRC, which include adenocarcinoma, mucinous adenocarcinoma, and signet ring cell CRC, our current studies focused on CRC adenocarcinoma given its high prominence (65.20%) according to a metanalysis study conducted earlier in this project using TCGA COAREAD cohort dataset (Figure 1).

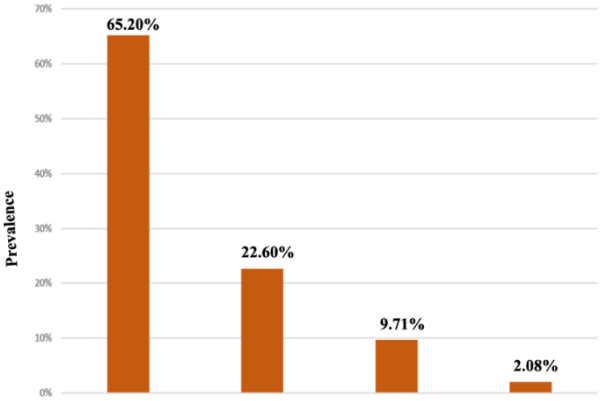

Figure 1 - CRC histological subtypes and their prominence. Classification and Prominence of CRC subtypes at the primary site in the cohort TCGA COAREAD samples; n= 736. UCSC Xena Browser was used for graph generation and dataset access [19].

Adenocarcinomas are solid glandular tumors derived from mucus-producing glands with a three-years higher prognosis than the mucinous rare CRC subtype, particularly due to the lack of mucinous vacuoles, which facilitate lymph nodes infiltration and metastasis [5]. In general, stages of CRC begin with the intramucosal carcinoma (stage 0). At this stage, the polyps are still maintained in the innermost mucosa layer of the colon or rectum. Then, stage 1 of CRC occurs when the tumor grows through the muscularis mucosa reaching the submucosa. Afterwards, stage 2 is divided into three sub-stages: IIA, IIB, IIC, indicating how far into and through the outermost layer of the colon, muscularis propria, or rectal wall the tumor has reached. By IIC, the tumor penetrates the colon/rectal wall and attaches to nearby tissues and organs. Similarly, stage 3, is divided into three stages that include: IIIA, IIIB, IIIC, which also indicate the extent and number of lymph nodes and fat tissues which the tumor had invaded, with C being the most invasive one. Finally, stage 4, marks the farthest metastatic site the CRC tumor has reached. For example, in substage IVA, the tumor will have spread to one distant organ or set of lymph nodes, while in IVB, the tumor has reached to more than one distant organ, ending with the most advanced substage IVC where the CRC tumor has spread beyond the peritoneum and past the abdominal cavity [6].

The chronological, yet complex progression of CRC, along with the interdependency on its surrounding microenvironment increases the difficulty to effectively tackle the tumor without interfering with the cell cycle of normal cells in the vicinity of the tumor. Directly targeting the tumor itself using tumor suppressive and angiogenesis blocking drugs, have repetitively failed to pass clinical trials [7]. This sheds light on the importance of elucidating the reciprocal interactions that occur between the tumor cells and its surrounding microenvironment. The tumor microenvironment encompasses the stroma, consisting of a basement membrane

that defines the tumor epithelial cell compartment, fibroblasts, extracellular matrix, immune cells, and endothelial cells lining the vasculature [8]. Two types of fibroblasts usually reside in the tumor's microenvironment: naïve fibroblasts and cancer associated fibroblasts (CAF). Naïve fibroblasts are typically responsible for secreting extracellular matrix (ECM) components, such as collagen and fibronectin to form the basement membrane. They are also essential secretory cells that produce soluble paracrine and autocrine growth factors required for cell-cell communication with the surrounding growing cells [8]. Fibroblasts' crucial role not only lies in their structural function, but rather in their ability to remodel the ECM to best fit the needs of the cell types in a specific tissue.

We outlined in Figure 2 one of the suggested bi-directional mechanisms that were derived from studies done by Peng et. al. [9]. As shown, the process begins with the tumor cells secreting a latent transforming growth factor that is associated with the latency-associated peptide (TGF-β-LAP) into the ECM. Removal of the LAP from the TGF-β-LAP complex occurs through the binding of the αv motif in αvβ6 integrin to an RGD sequence present in the LAP [10]. TGF-β, now in its active form, mediates the reprogramming of the naïve fibroblasts to CAF. The crosstalk between the tumor cells and the CAFs continues with the CAF secreting stromal cell-derived factor-1 (SDF-1), which in return facilitates a chemotactic gradient that allows the tumor cells to metastasize to organs expressing SDF-1 receptors. This eventually promotes a migratory and an invasive phenotype.

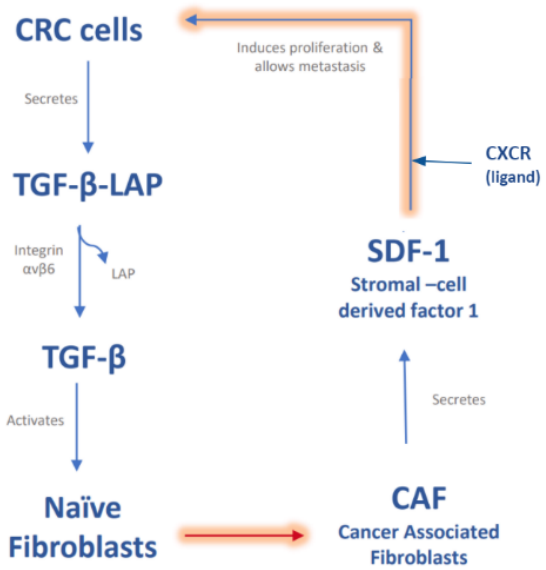

Figure 2 – Crosstalk between CRC and CAF. The relationship schema displays how the colorectal cancer cells (CRC) initiate the reprogramming of naive fibroblasts to cancer associated fibroblasts (CAF) and thus promoting tumor growth.

While the suggested mechanism is one of many, the schematic presented in Figure 2 is displayed as a rough draft of the circuit to help identify the research gaps. The highlighted orange arrow indicates our interest in these pathways. It is important to note that the suggested TGF-β reprogramming pathways is one of many other possible ones, and that although it is adapted in this research it not restricting. In other words, NF to CAF reprogramming can happen using other signaling pathways as well.

The difference between naïve fibroblasts and CAFs will be established by characterizing naïve fibroblasts before and after co-culturing with the CRC cell line, HCT-116. HFF cells, also known as human foreskin fibroblasts, are primary adherent cell line readily used for its availability and convenience compared to organ specific fibroblasts [10]. The CRC immortalized cell line HCT-116 derived from a male patient with malignant CRC tumor are adherent and cuboidal in morphology [11]. While HCT-116 has been characterized to express the multifunctional cytokine TGF-β, in return, the chosen HFF cell line has been confirmed to express the TGF-β receptor [12]. Thus, TGF-β paracrine signaling can occur between the two cell lines, enabling the naïve fibroblasts to get transformed to CAF. Next, to determine the difference between the two types of fibroblasts and further identify the reprogrammed ones, the hallmark marker α-smooth muscle actin (α-SMA) will be used to identify the CAF subpopulations [9]. In addition, the pro-inflammatory signature chemokines CCL-8 will be examined given it is known ability to attract other immune cells such as monocytes

and lymphocytes to enhance adhesion, migration, and invasion levels of the surrounding tumor; especially to the liver [14]. Hence, if the expression of CCL-8 and α-SMA are upregulated in the supposedly CAF, then we can suggest that the reprogramming of the anti-inflammatory naïve fibroblasts to the pro-inflammatory CAF has indeed occurred.

To replicate the in vivo conditions where the tumor cells and the fibroblasts are in close vicinity, HCT-116 cells will be cultured as 3D spheroids where the polarity and integrity of the cells is not compromised and by addition of the fibroblasts to the spheroid structures. In addition, HFF cells will be studied on a collagen coated 2D plates to characterize whether a difference in their growth and behavior is present compared to how they are expected to behave in vivo and to evaluate the role of the ECM in triggering the transition from a naïve phenotype to CAF populations.

Methodology

Cell Culture. HCT-116 cells (ATCC® CCL-247™) were maintained in a culture medium consisting of McCoy's 5a Medium Modified, 10% Fetal Bovine Serum (FBS), and 1% (100 U/ml) Penicillin-Streptomycin mixture. Seeded cells were incubated in a humidified incubator with 5% carbon dioxide at a temperature of 37°C, where the culture medium was changed every 2-3 days as needed. At 80% confluence, cells were resuspended and passaged at a 1:8 ratio. HFF cells, previously purchased from (ATCC® SCRC-1041™), were kindly provided by Sidra Medicine, Qatar, and were maintained in similar conditions as mentioned above, however, Dulbecco's Modified Eagle Medium was used (DMEM).

Spheroid Volume to Cell Count Experimental Design.

HCT-116 3D Culture. Nunclon™ Sphera™ ultra-low attachment 96-well plate was used to seed HCT-116 cells at different cell densities per well: 1.5 x 10^4, 3.0 x 10^4, and 6.0 x 10^4 cells/ 200 µl. This plate type was used in an endeavor to grow the cells in suspension with virtually no cell attachment. That is because the ultra-low attachment plate allows the cells to grow in natural, repeatable manner mimicking the in vivo organization. After seeding, cells were incubated in a humidified air incubator with 5% Co_2/ 95% air at a temperature of 37°C. Imaging of all cell-containing wells was done using EVOS FL Life Technologies Cell imager under normal light at two objectives: 4X and 10X every 24 hrs.

Volume Analysis (growth curve). Using ImageJ Software ((National Institutes of Health, Bethesda, MD, USA) the diameters of the imaged spheroids were measured. For each spheroid, a vertical and horizontal diameter was measured, an average diameter was calculated and used to find the radius and then calculate the volumes of the spheroids using the following equation $v_{Sphere} = {}^{4}/_{3}\ \pi r^3$. All cell densities seeded were done in octuplicates (n=8) and standard deviation was considered.

Trypsin titration and spheroid dissociation. Titration of trypsin was conducted where TrypLE™ Express (REF: 12605-010) was diluted at a ratio 1:10 and 1:100 using sterile PBS. Each concentration of TrypLE was separately used with for spheroid dissociation for three incubation periods 5, 10 and 15 minutes. The optimum conditions for an efficient spheroid dissociation without compromising the viability of the cells was incubating the physically agitated spheroid in 50 µl of 100x diluted TrypLE for 15 minutes in the humidified incubator with 5% carbon dioxide at a temperature of 37°C.

Counting. 10 µl of the dissociated spheroid were mixed with 10 µl of Trypan blue to assess for cell viability and counted using a hemocytometer with the cell count calculated as the following: Cell count = average count of the hemocytometer's 4 corners x 10^4 x 2 (accounting for the trypan blue dilution).

Enzyme-linked immunosorbent assay (ELISA) to check for the expression of CCL8.

3D culture of HCT-116, HFF, and co-culture. For this experiment HCT-116 and HFF cells were seeded separately at a density of 15,000 cells/well using ultra-low attachment 96 well plates, another set of HCT-116 cell lines were seeded at the same density to collect conditioned medium (CM), and finally a co-culture of HCT-116 and HFF at a 1:2 ratio was established, with the total number of cells maintained at 15,000 cells per well. After 24 hours, 150 ul of the media of the second set of HCT-116 was replinshed with 150 ul of fresh 5% FBS McCoy media (leaving 50 ul of original media in the well), and then collected and swapped after 24 hours such that we culture HCT-116 HFF growing in HCT-116 CM. This was done to identify the directionality and effect of the secreted chemokines.

Sample preparation. From each condition: HCT-116 alone, HFF alone, co-culture, HFF and HCT-116 CM, 150 ul of the medium was collected and centrifuged for 20 minutes at 1000xg at 4 ℃, then added to the in 100 ul aliquots to the precoated 96 well micro-ELISA plate.

Assay. The protocol was adapted from Novus Human CCL8/MCP-2 ELISA Colorimetric Kit (NBP2-68059) to prepare all required working solutions. The standards were prepared following the protocol with a serial dilution gradient of 400, 200, 100, 50, 25, 12.5, 6.25, 0 pg/mL, and then added to the ELISA plate at 100 ul aliquots and in duplicates. The standards and collected medium could interact with the CCL-8 antibody on the wells' matrix for 90 min at 37 ℃, then treated with 100 ul of biotinylated detection antibody working solution and incubated for 60 min at 37℃ to allow the introduced secondary antibody to bind to the coated first CCL8 antibody. Afterwards, all wells were washed with 350 ul of wash buffer three time and Avidin-Horseradish Peroxidase (HRP) conjugate was added to each well in the microplate to tag the second biotinylated antibody during a 30 min incubation at 37 ℃. After that, five washes were conducted as previously described and 90 ul of substrate reagent was added in the dark and incubated for 15 min at 37 ℃ to allow for the development of the colorimetric reaction. The development was then stopped with 50 ul of stop solution. The optical density (O.D) was measured spectrophotometrically in a microplate reader at 450 nm from which the concertation of CCL8 was calculated in relevance to the standard curve.

Fluorescence-activated single cell sorting (FACS) to measure the expression of Integrin αvβ6.

Sample preparation. HCT-116 sample cells and positive control MCF7 breast cancer cells were washed, trypsinized, pelleted, resuspended in 1 ml of plain media (McCoy for HCT-116, and DMEM for MCF7), and counted using hemacytometer to ensure that each FACS tube contains 1.0×10^6 cells (changing from provided protocol developed in Dr. Bouaouina's lab to accommodate for assumed cell loss). Six total tubes were prepared: a set of each cell line would contain no antibodies, another set would only contain the secondary antibody, and a third set which would be the sample one containing both the first and secondary antibody.

Assay. One set of the FACS tubes containing 1 million cells of each cell type were each resuspended in 0.5 µl PBS and set aside to serve be used to subtract any fluorescence emitted by the cells themselves: negative control. Then, another set of FACS tubes containing cells was treated with 1:200 plain DMEM diluted primary antibody: Mouse Anti-Integrin αVβ6 Antibody, clone 10D5, azide free [MAB2077Z], incubated at 4 ℃ for 30 min, then centrifuged for 5 min at 1300 rpm. Following that the primary antibody treated set and the remaining set were treated with 1:300 plain DMEM diluted secondary antibody: Goat anti-Mouse IgG (H+L) Cross-Adsorbed Secondary Antibody [A-21235], incubated at 4 ℃ for 30 min, incubated at 4 ℃ for 30 min, then

centrifuged for 5 min at 1300 rpm. Both sets of stained pellets were eventually resuspended in 0.5 ml of PBS. All samples were analyzed using BD ISRFortessa Flow Cytometer.

Clinical colon tissue samples. Clinical pathological and normal colon tissue cells embedded in paraffin tissues were purchased from Novus biologicals. Tissues were obtained at a 5 μm thickness and mounted to frosted slides. Normal colon fixed, dehydrated, and paraffin infiltered tissue biopsy was obtained from a 60-year-old male. An adenocarcinoma obtained from a 41-year-old female was also used. In addition to a mucinous adenocarcinoma taken from a 44-year-old male patient. As for the microarray, 29 colon tumor/adjacent normal pairs were treated on the same slide with no patient's information provided. All clinical samples were subjected to Trichrome staining. Trichrome stained samples were imaged at 4x, 10x, and 20x objectives using the inverted Zeiss Axio Scope A1 light microscope.

Clinical Samples Immunofluorescence Staining. To localize the expression of α-SMA in clinical samples, tissues were deparaffinized with xylene and then gradually rehydrated through 100%, 90%, and 70% alcohol. Antigen retrieval was performed using the Citrate buffer (pH = 6.00). Tissues were then blocked with 1x PBS containing 5% FBS and 0.3% TritonX-100 for 1 hour at room temperature to avoid nonspecific antibody binding. Tissues were washed with PBS and then incubated overnight at 4℃ with 1:200 PBS diluted primary antibody (mouse anti- α-SMA). Another wash was conducted followed by a 1-hour incubation at room temperature with the secondary antibody (goat anti-mouse secondary antibody conjugated with Alexa Fluor 555). DAPI staining solution was added for 30 min as a final step to localize nuclei and the overall architecture of the tissue, before mounting the tissues with an anti-fade reagent.

Results

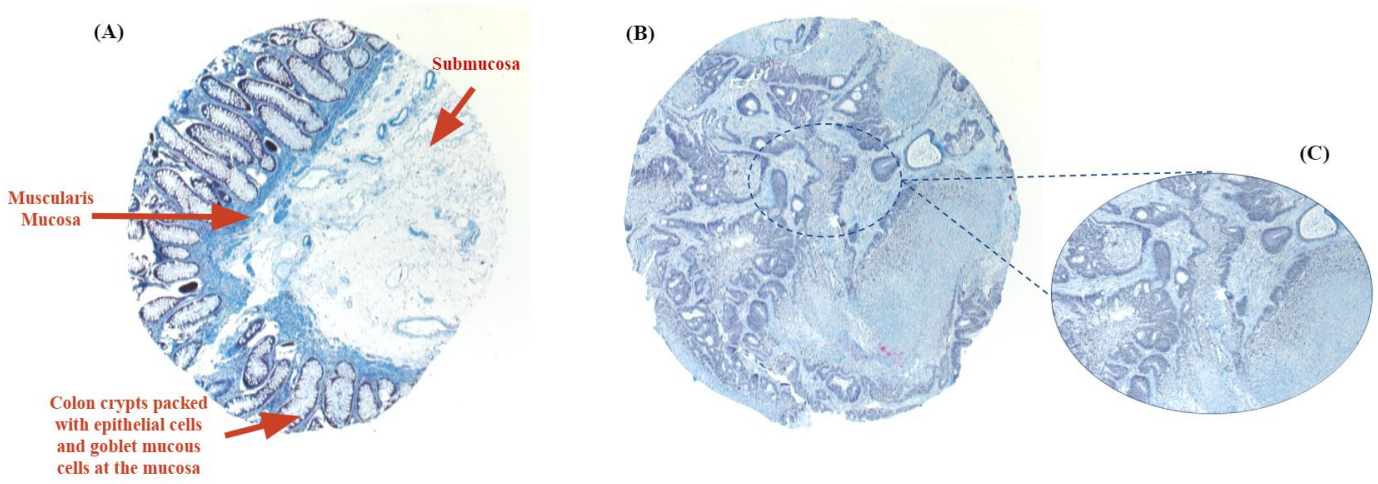

Figure 3 - Normal Colon Tissue in adjacence with CRC Adenocarcinoma. Two representative images of trichrome staining were chosen from a microarray panel of 29 adjacent tumor/normal pairs. **(A)** Normal colon tissue microscopic image taken at 4x objective showing defined boundaries between the layers of the colon wall where the layerc ontaiing the epithelial cells is clearly separated from the submucosa by the muscularis mucosa **(B)** CRC adenocarcinoma microscopic image at 4x objective displaying complete infiltration of the stroma by tumor cells, displaying a disorganized histological architecture. (C) Inset depicting not only the migration of tumor cells into the surrounding stroma, but also the recruitment of immune cells, indicating the prevalence of an inflammatory immune response in the tumor microenvironment (20x).

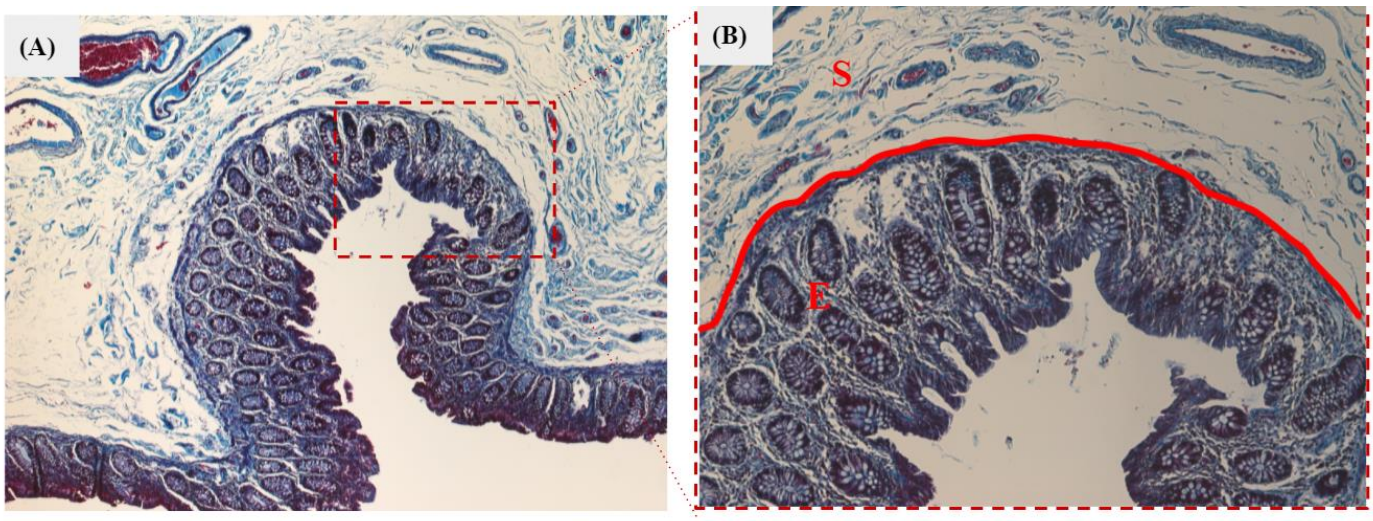

Figure 4 - Normal Colon Tissue. (A) Normal colon wall histology image at 4x objective from a 60-year-old male patient showing the segregated layers of mucosa, submucosa, and muscularis. **(B)** Microscopic image at 20x objective of the outlined area displaying the regular organization of the goblet and epithelial cells in the mucosa with a basal membrane (in red) separating the mucosa from the muscularis layer; E = epithelial cells, S = Stroma.

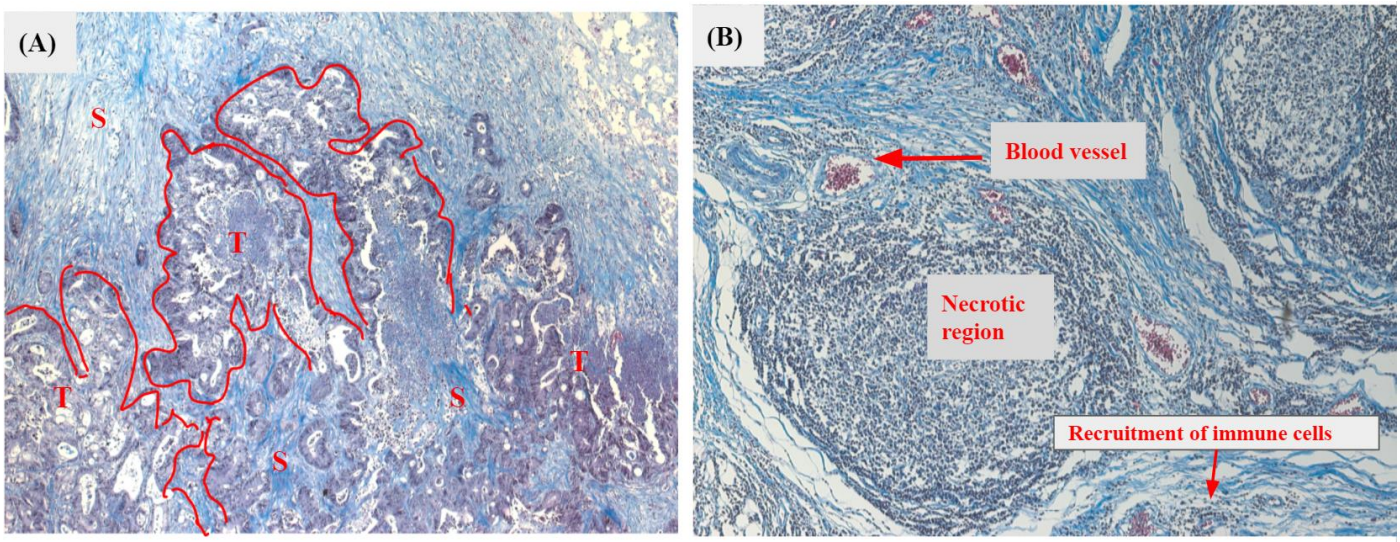

Figure 5 - Histopathology of CRC subtypes. Two representative microscopic images of **(A)** CRC adenocarcinoma from 41 years old female and **(B)** mucinous CRC adenocarcinoma clinical sample from a 44-year-old male patient, taken at 10x objective. Both images display the distorted organization of the colon lining in relative to its surrounding stroma. T = tumor cells, S = stroma.

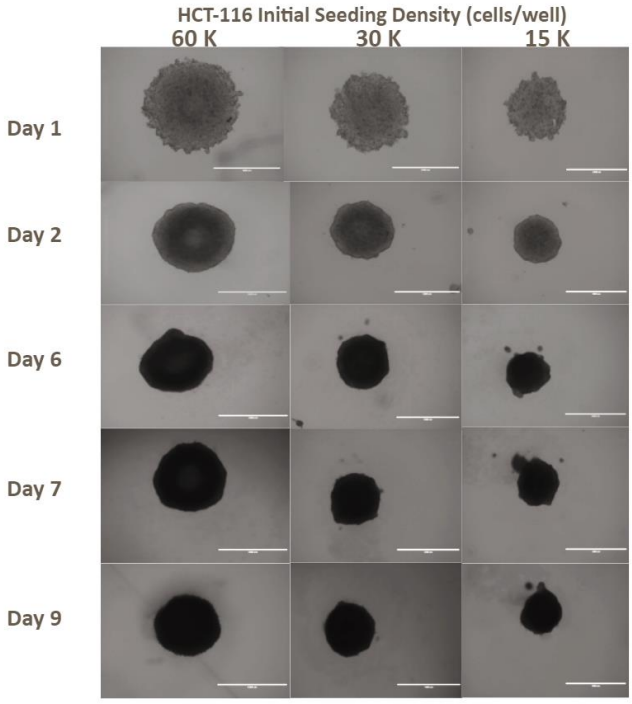

Figure 6– HCT-116 3D Spheroids Formation. Images of spheroids at 4X magnification were taken to monitor the development of spheroids seeded at varying initial seeding density of 60 x 10^3, 30 x 10^3, and 15 x 10^3 cells per well. Scale bar: 1000 µm.

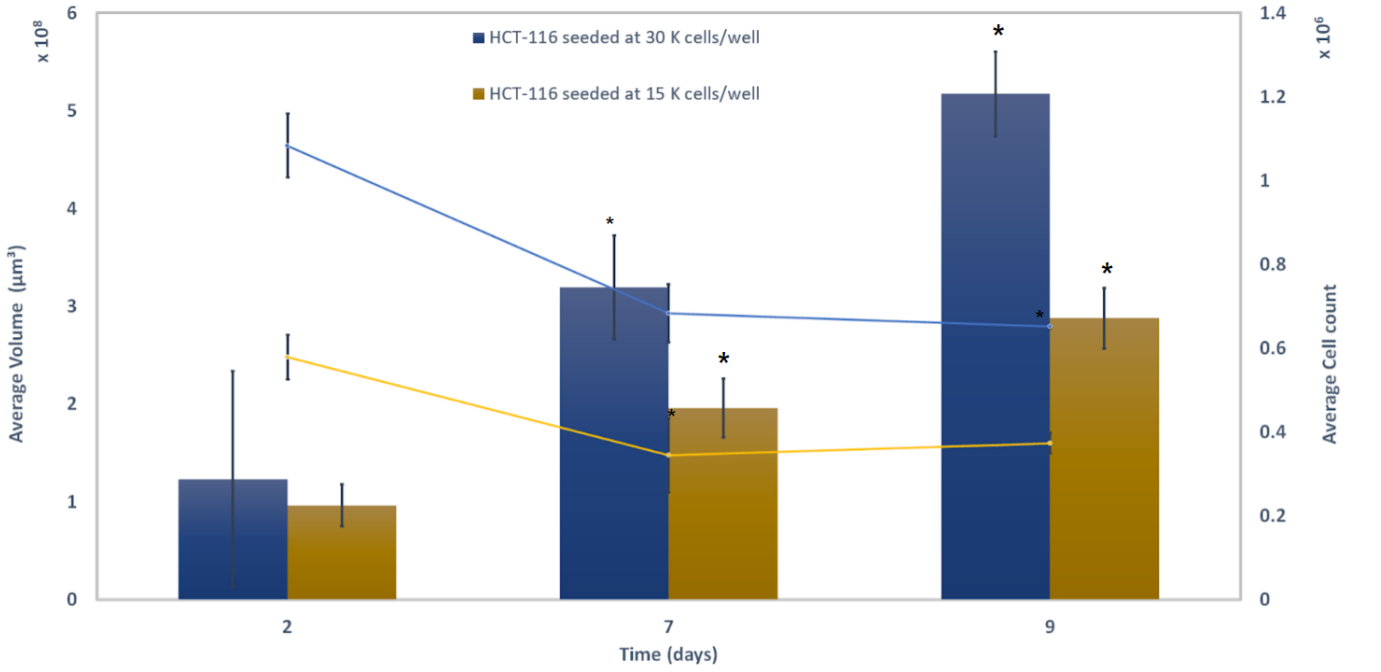

Figure 7 - Rate of Average Volume and Cell Count change of HCT-116 3D spheroids. HCT-116 spheroids were cultured for 9 days at which three spheroids of each seeding density 30, 000 cells/well and 15,000 cells/well were imaged at 4x objective using inverted light microscope, dissociated with 10x TrypLE™ diluted in PBS, and the single cell suspensions were counted using a hemocytometer. An inverse correlation between volume and average cell count is observed.

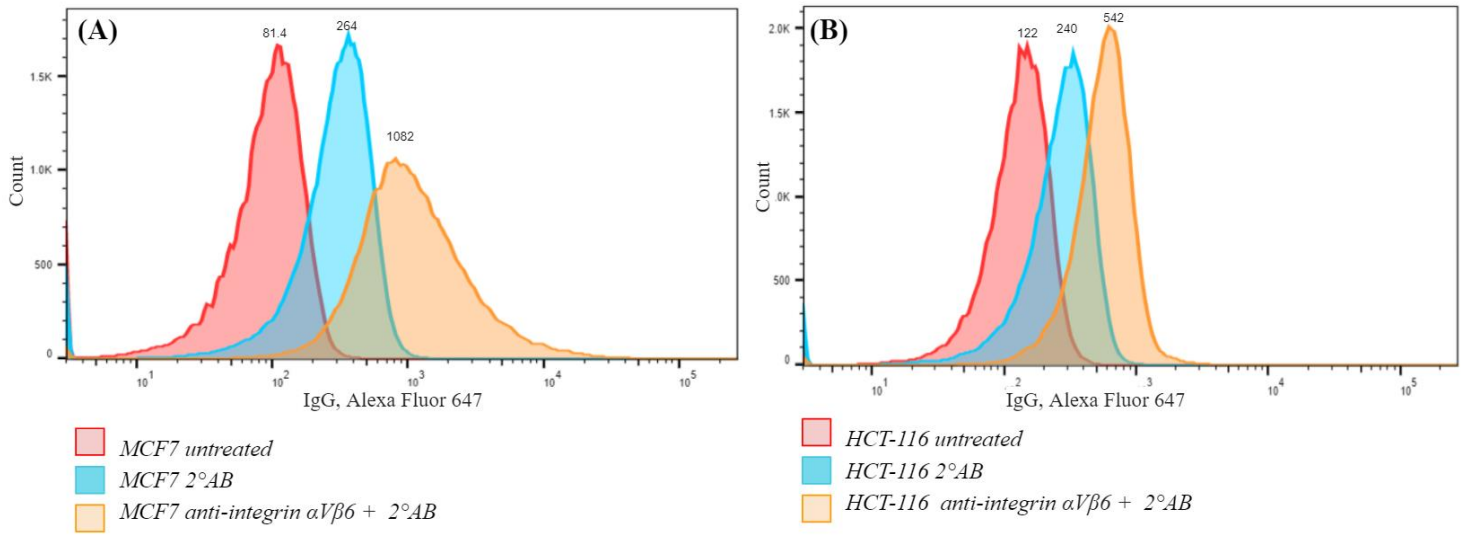

Figure 8 - Fluorescence-activated cell sorting (FACS) results for the expression of integrin αVβ6. MCF7 (A) and HCT-116 (B) cells were labeled with mouse anti-integrin αVβ6 antibody and tagged with goat anti-mouse IgG cross-adsorbed secondary antibody Alexa Fluor 647. Results were acquired using the BDlSRFortessa Flow Cytometer and analyzed using FlowJo (orange peaks). Controls for each cell line included cells without incubation with any of antibodies (untreated cells, red peaks)) and cells that were incubated with the secondary antibody alone (2° Ab; blue peaks).

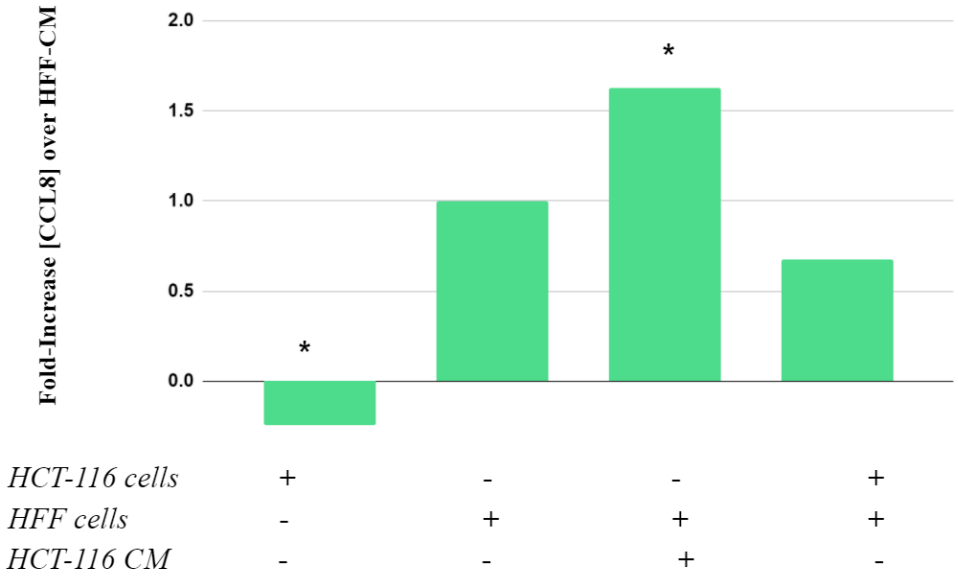

Figure 9 - Fold increase of CCL-8 expression over HFF conditioned medium (CM). Levels of secreted CCL8 were evaluated in media collected from the wells containing HCT-116 spheroids alone, media from HFF spheroids alone, and media of 24 hours incubated HCT-116 CM with HFF spheroids. The stained media were prepared in accordance with the ELISA kit protocol (NBP2-68059) and the absorbance was measured at a wavelength = 450 nm. The CCL8 concentrations of each condition was calculated using the equation $y = 0.0102x + 0.5578$, $R^2 = 0.9038$ obtained from a standard curve of duplicate standards measurements. Results were plotted as the fold increase ratio of each experimental condition over the CCL8 levels in the media of HFF alone, hence no error bars representing standard deviation are added; n = 3; *t-test $p < 0.05$; noting that all (*) values plotted are significant compared to HFF CM alone.

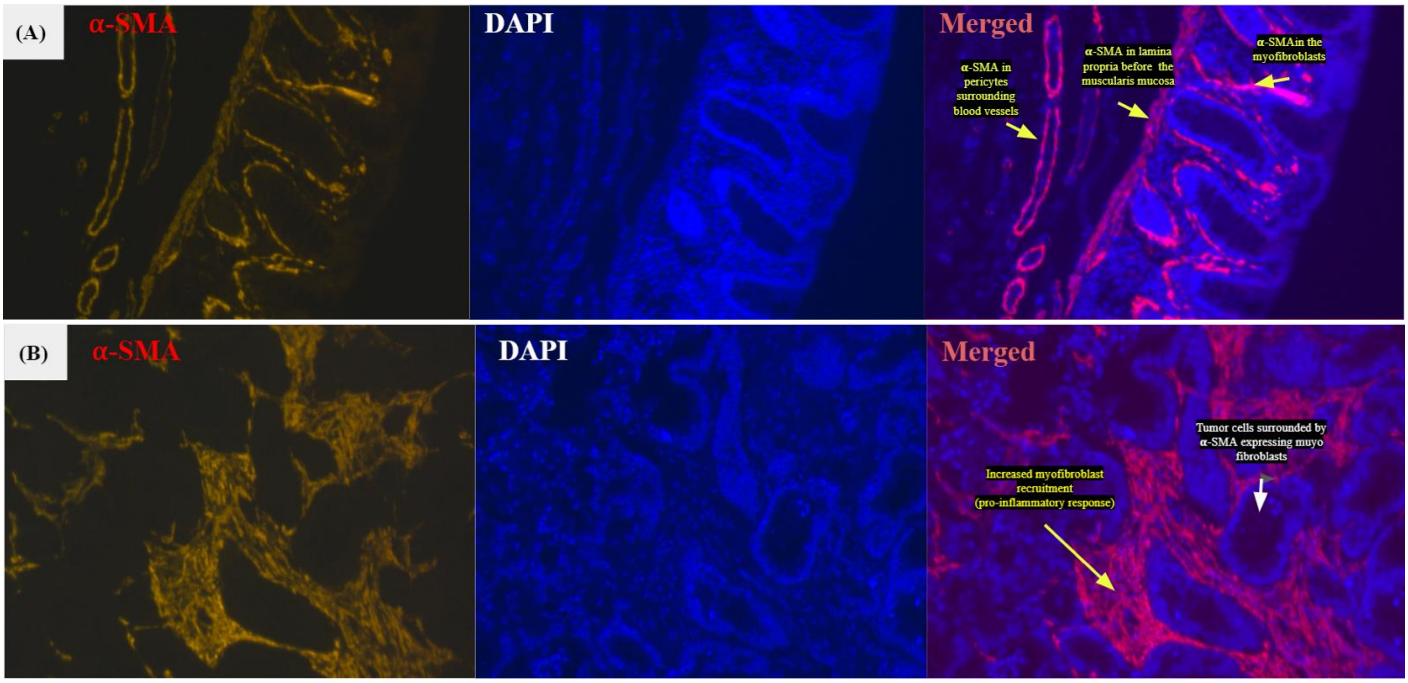

Figure 10 - *α*-SMA and DAPI immunostaining. (A)Normal colon tissue from 60 years old male patient and **(B)** colon adenocarcinoma from a 41-year-old female were deparaffinized in xylene, rehydrated with alcohol, their antigen retrieved with citrate buffer, blocked 1x PBS containing 5% FBS and 0.3% Triton, and then stained with mouse anti-***α***-SMA, and goat anti-mouse secondary antibody conjugated with Alexa Fluor 555. Samples were also stained with DAPI for gross tissue morphology analysis. Samples were imaged using inverted microscope with red and blue filters and then overlapped with ImageJ software.

Discussion & Conclusions

Cellular to Tissue Linkage:

As shown in Figure 3 using the representative adjacent normal/ tumor tissue, the architecture of the tissue in the normal colon (3A) is organized the lamina propria separates the epithelial layer containing the organized cells from the muscularis propria and the submucosa. However, in Figure 3B we see that the separation between the layers became distorted around the invasive tumor cells. The trichrome staining displays the infiltration of the stroma with fibroblasts and collagen deposits as a difference in stain color where the ECM (containing collagen) was stained in blue in contrary to the epithelial and cancerous cells stained in purple. A closer look of this infiltration is apparent in Figure 5A where the epithelial cells boundary is lost given that the tumor cells are seen growing uncontrollably beyond the epithelial layer. The effect of the CRC cells on its stroma is highlighted in Figures 4 and 5. Figure 5 depicts how the microenvironment surrounding the tumor is altered with some evidence of hypoxia and pro-inflammatory response. This is inferred from the presence of the necrotic area observed in Figure 5B and the recruitment of immune cells from the blood vessels.

These histological studies suggest that when modeling a tumor at a microscopic 3D culture level, the ratio of fibroblasts to tumor cells should be taken into consideration. This observation was noted and implemented when coculturing HCT-116 and HFF cells.

Testing Model Optimization:

The choice of adapting a 3D culture approach over 2D for tumor cells originates from the fact that a 3D culture allows for preservation of cellular polarity, gene expression, and the in vivo -like distribution of oxygen, nutrients, cytokines, and other signaling molecules. In addition, the cell-cell and cell-ECM interaction

of 3D culture are more integrated compared to cells grown in 2D [16]. Moreover, drug toxicity testing results has shown that 2D and 3D culture have totally different responses to drug toxicity as studied by the effect of tamoxifen on MCF-7 cells [17]. Hence, to better study the interaction of a potential drug in vitro prior to animal testing and clinical trial, 3D spheroid settings offer the closest model to a tumor in vivo. To better represent and study the progression of a 3D spheroid in parallel to in vivo tumors, seeding at different densities were evaluated as shown in Figure 6. As time increased, we observed that the size of the spheroids was decreasing while their compactness was increasing, as evaluated by the darkness of the spheroids. However, it was not clear whether this compactness relates to the enhanced proliferation of the cells within the spheroids or on the contrary, to the attenuation of their proliferation rates and loss of cells due to apoptosis. Our results show (Figure 7) that the volume and cell count of the spheroids are inversely correlated. We hypothesize that this can be a result of stronger cell-cell adhesion within the tumor cells in the spheroid and may also be due to an enhanced proliferation of these cells sue to paracrine factors secreted when aggregated in a spheroid structure. we also noticed that some tumor cells begin to migrate out of the spheroid itself (Figure 6). This could be due to the fact that cells within the central layers of the spheroids do not have same access to oxygen and nutrients compared to those located to the periphery of the tumor, hence triggering their movement away from the center of the spheroids. We suggest that we need to assess the viability of the tumor cells within the sheroids, for instance a Lactate dehydrogenase LDH release assay can be helpful to identify whether they are some of the necrotic cells within the spheroids or whether the cells acquired a migratory-like behavior. In conclusion, we suggest that spheroid volume may not be indicative of the spheroid growth status and that other proliferation and growth assays should be used. The volume of the spheroids can be used as a control when developing identical testing models however it should not be used on its own to evaluate growth rate.

Effect of Tumor Cells on Surrounding Stroma:

To understand the relationship in which the naïve fibroblasts are reprogrammed into CAF, some factors secreted by the surrounding tumor cells must be present. Indeed, TGF-β-LAP cannot be activated without the presence of integrin αVβ6 that is most likely expressed by the CRC HCT-116 cell line. Hence, we checked for the expression of integrin αVβ6 using flow cytometry. Results in Figure 8 reveal that there was an expression of integrin αVβ6 in HCT-116 cells, at levels that were similar to MCF-7 cells used a positive control. We note that the expression of integrin αVβ6 seems low, and we speculate that this may be due to the dilution of the antibodies in relative to the samples cell population. The number of cells processed was doubled compared to the protocol, which could have led to a decrease in expression level when being reported as a fraction of the total integrin expression in the sample. Likewise, there were no replicates conducted because the quantification of integrin expression was not the target of this experiment, the endeavor was checking for its presence or absence.

After confirming the presence of integrin αVβ6 by flow cytometry and taking into consideration previous studies reporting TGF-β secretion by HCT-116 cells [12], we next sought to evaluate the reprogramming of naïve fibroblasts to CAF by the tumor cells. To address this, the chemokine CCL8 was chosen as it has been known as a pro-inflammatory signature marker secreted by CAF. CCL8 secretion has been previously shown to enhance adhesion and migration of the surrounding tumor cells site [15]. Indeed, in Figure 9, we saw a significant fold increase in the secretion of CCL8 in the media of the HFF spheroids which has been exposed to HCT-116 CM compared to the media collected from HFF spheroids growing in their own

media. These results suggest that there are factors secreted by the HCT116 spheroids, which upon incubation with HFF-derived spheroids, enhanced the secretion of CCL8 from the HFF cells. In conclusion, we suggest that the interaction of naïve fibroblasts with factors secreted by the tumor cells may activate the fibroblasts into CAFs. Although we did not observe an increase in secretion of CCL8 in spheroids derived from HCT116 and HFF co-cultures, we speculate that when cells are in direct contact with each other, longer incubation time may be required to see an effect.

Finally, we sought to identify and compare the aggressiveness of fibroblasts in normal colon tissue compared to reprogrammed fibroblasts, CAF, in the pathological adenocarcinoma colon tissue sample. The marker α-SMA was chosen to identify CAFs from NF as it is upregulated in activated myofibroblasts and is also expected to be enhanced in CAF. As portrayed in Figure 10 (A) the merged image shows how α-SMA is normally expressed in the smooth muscles of the lamina propria separating the mucosa from the muscularis propria and around blood vessels. However, in Figure 10 (b) we observe the complete prevalence of α-SMA-positive cells in the stroma surrounding the tumor cells. While we acknowledge that this increase may be attributed to the reprogramming of resident fibroblasts, vimentin expression (housekeeping protein in fibroblasts in general) should be done to co-localize α-SMA expression to fibroblast populations in the stromal compartment.

Conclusion and Future Works

We conclude that tumor cells play a role in reprogramming of naïve fibroblasts to CAF by secreting a myriad of cytokines that activate the fibroblasts to become pro-inflammatory. The activation of the fibroblasts in return mediates a pro-inflammatory response by possibly recruiting immune cells from nearby blood vessels and thus, contributing to tumor progression down a chemotactic gradient. Moreover, the model optimizations experiments highlight that the best seeding density is around 30×10^3 cells/well and that the tumor spheroids should be analyzed within one week following the initial seeding or that the media should be regularly changed to avoid the distortion of the spheroids overtime. In addition, while the cells in the spheroid are proliferating and increasing the cell count, the spheroid size is shrinking in return indicating that the spheroid is becoming denser but not necessarily mimicking a tumor growth; hence other growth rate analysis must be conducted. At last, the link between studying CAF in tissue histology and at the cellular level using spheroid structures works in parallel to recapitulate the microenvironment in which the tumor thrives.

As a next step, the effect of the CAF on the tumor cells should be investigated by incubating an HCT-116 spheroid with HFF conditioned media for 24 hrs, then the media will be collected and analyzed for for markers of proliferation aggressive such as interleukin-6 and 10 using RT-PCR. Moreover, further analysis should be done to confirm the levels of activated TGF-β by the integrin αvβ6 expressed by the HCT116 cells, and that can be done by incubating the latent form TGF-β-LAP with HCT-116 cells for 24 hours and then collecting the media and performing an immunological assay such as ELISA to detect the activated form [9]. We also believe that other reprogramming pathways could be explored to compare whether the same markers and cytokines are expressed/generated when NF become activated to CAF.

Appendix:

Example of the results from measuring activated activated TGF-β as described in future results.

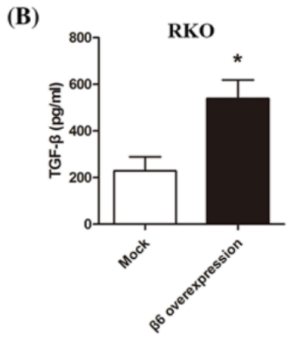

Figure (3B; Peng et. al) ELISA show TGF-β levels in the culture media collected from mock transfected (Mock) RKO CRC cells and β6 transfected (β6 overexpression) RKO CRC cells. Accompanying the increased expression of β6, TGF-β levels increased significantly (*P<0.05).

Effect of integrin avβ6 on CAF (Peng et.al)

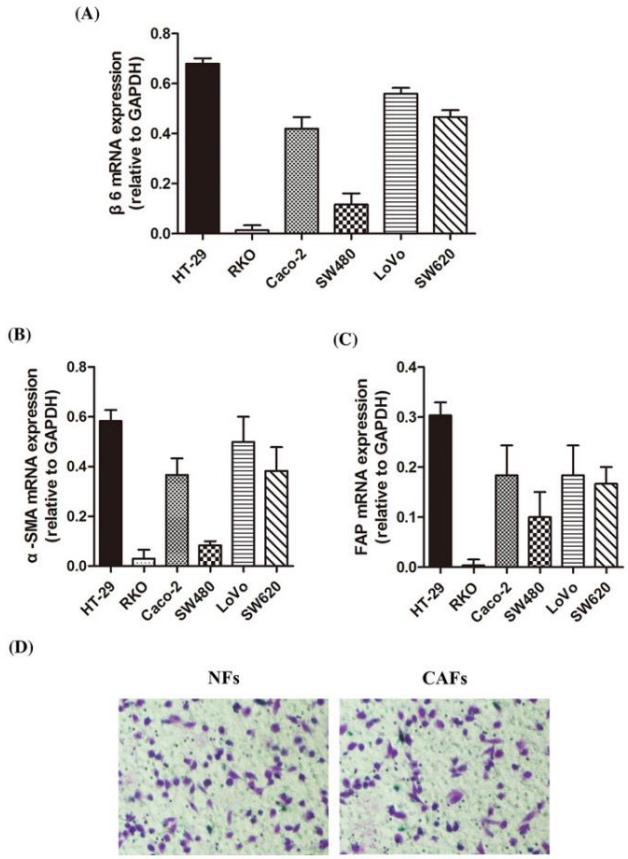

Figure 1. Integrin αvβ6 is expressed in CRC cell lines and promotes the activation of fibroblasts
(**A**) RT-PCR assay shows *β6* mRNA expression in six types of CRC cell lines. (**B**) RT-PCR assay shows α-*SMA* mRNA expression in the media collected from CCD-18Co cells co-cultured with the above-mentioned CRC cell lines. (**C**) RT-PCR assay shows *FAP* mRNA expression in the media collected from CCD-18Co cells co-cultured with the above-mentioned CRC cell lines. (**D**) Invasion experiment shows no difference observed between CAFs activated by cancer cells and those without cancer cells pretreatment. Data are mean ± S.E.M. from three independent experiments.

References:

1. Siegel, R. L., Miller, K. D., Goding Sauer, A., Fedewa, S. A., Butterly, L. F., Anderson, J. C., ... & Jemal, A. (2020). Colorectal cancer statistics, 2020. *CA: a cancer journal for clinicians.*
2. World Health Organization. (2014). *Cancer Country Profile - Qatar* (Rep.).
3. Potter, J. D. (1999). Colorectal cancer: molecules and populations. *Journal of the National Cancer Institute*, *91*(11), 916-932.
4. Coppedè, F., Lopomo, A., Spisni, R., & Migliore, L. (2014). Genetic and epigenetic biomarkers for diagnosis, prognosis and treatment of colorectal cancer. *World journal of gastroenterology*, *20*(4), 943–956. https://doi.org/10.3748/wjg.v20.i4.943
5. Luo, C., Cen, S., Ding, G., & Wu, W. (2019). Mucinous colorectal adenocarcinoma: clinical pathology and treatment options. *Cancer communications (London, England)*, *39*(1), 13. https://doi.org/10.1186/s40880-019-0361-0
6. Colorectal Cancer Stages. (2018). Retrieved May 01, 2020, from https://www.cancer.org/cancer/colon-rectal-cancer/detection-diagnosis-staging/staged.html
7. Wang TJ, Carpenter D, Lauffenburger JC, Wang B, Franklin JM and Kesselheim AS: Failure of investigational drugs in late-stage clinical development and publication of trial results. JAMA Intern Med 176: 1826-1833, 2016.
8. Bremnes, R. M., Dønnem, T., Al-Saad, S., Al-Shibli, K., Andersen, S., Sirera, R., ... & Busund, L. T. (2011). The role of tumor stroma in cancer progression and prognosis: emphasis on carcinoma-associated fibroblasts and non-small cell lung cancer. *Journal of thoracic oncology*, *6*(1), 209-217.
9. Peng, C., Zou, X., Xia, W., Gao, H., Li, Z., Liu, N., ... & Fang, R. (2018). Integrin αvβ6 plays a bi-directional regulation role between colon cancer cells and cancer-associated fibroblasts. *Bioscience reports*, *38*(6).
10. ATCC. (n.d.). HCT 116 (ATCC® CCL-247™). Retrieved April 28, 2020, from https://www.atcc.org/products/all/CCL-247.aspx
11. HFF-1 (ATCC® scrc-1041™). (n.d.). Retrieved April 11, 2021, from https://www.atcc.org/products/all/SCRC-1041.aspx
12. Clement, C. A., Ajbro, K. D., Koefoed, K., Vestergaard, M. L., Veland, I. R., de Jesus, M. P. R. H., ... & Christensen, S. T. (2013). TGF-β signaling is associated with endocytosis at the pocket region of the primary cilium. *Cell reports*, *3*(6), 1806-1814.
13. Shi, M., Zhu, J., Wang, R., Chen, X., Mi, L., Walz, T., & Springer, T. A. (2011). Latent TGF-β structure and activation. *Nature*, *474*(7351), 343–349. https://doi.org/10.1038/nature10152
14. Harper J, Sainson RC. Regulation of the anti-tumour immune response by cancer-associated fibroblasts. *Semin Cancer Biol* (2014) **25**:69–77. doi:10.1016/j.semcancer.2013.12.005
15. Torres S, Bartolome RA, Mendes M, Barderas R, Fernandez-Acenero MJ, Pelaez-Garcia A, et al. Proteome profiling of cancer-associated fibroblasts identifies novel proinflammatory signatures and prognostic markers for colorectal cancer. *Clin Cancer Res* (2013) **19**:6006–19. doi:10.1158/1078-0432.CCR-13-1130
16. Nyga, A., Cheema, U., & Loizidou, M. (2011). 3D tumour models: novel in vitro approaches to cancer studies. *Journal of cell communication and signaling*, *5*(3), 239.
17. Lv, D., Hu, Z., Lu, L., Lu, H., & Xu, X. (2017). Three-dimensional cell culture: A powerful tool in tumor research and drug discovery. Oncology letters, 14(6), 6999–7010. doi:10.3892/ol.2017.7134
18. Friedrich J, Eder W, Castaneda J, Doss M, Huber E, Ebner R, Kunz-Schughart LA. A reliable tool to determine cell viability in complex 3-d culture: the acid phosphatase assay. J Biomol Screen. 2007 Oct;12(7):925-37. doi: 10.1177/1087057107306839. Erratum in: J Biomol Screen. 2007 Dec;12(8):1115-9. PMID: 17942785.
19. Goldman, M.J., Craft, B., Hastie, M. et al. Visualizing and interpreting cancer genomics data via the Xena platform. Nat Biotechnol (2020). https://doi.org/10.1038/s41587-020-0546-8